Russian Physics Journal

COUNTRY	SUBJECT AREA AND CATEGORY	PUBLISHER	H-INDEX
United States Universities and research institutions in United States	Physics and Astronomy └ Physics and Astronomy (miscellaneous)	Springer New York	25

PUBLICATION TYPE	ISSN	COVERAGE	INFORMATION
Journals	10648887, 15739228	1992-2003, 2005-2021	Homepage How to publish in this journal physics@mail.tsu.ru

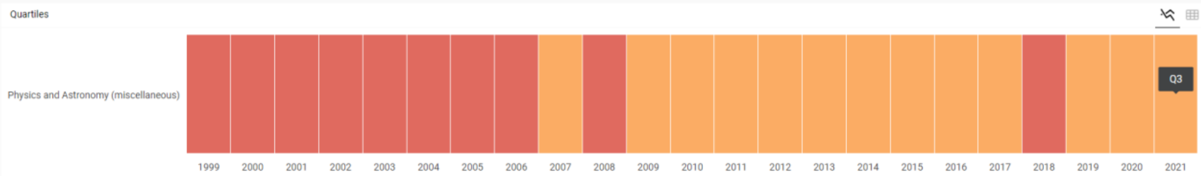

DOI 10.1007/s11182-022-02509-4

Russian Physics Journal, Vol. 64, No. 9, January, 2022 (Russian Original No. 9, September, 2021)

DEFORMATION AND FRACTURE OF HIGH ENTROPY AlCoCrFeNi ALLOY

Yu. F. Ivanov,[1] V. E. Gromov,[2] K. A. Osintsev,[2,3] S. V. Konovalov,[2,3] I. A. Panchenko,[2] and S. Chen[2,4]

UDC 669.017.15

Wire arc additive manufacturing in pure argon is used to fabricate the high entropy alloy system Al–Co–Cr–Fe–Ni *of the nonequiatomic composition:* Al *(35.67±1.34) at.%,* Ni *(33.79±0.46) at.%,* Fe *(17.28±1.83) at.%,* Cr *(8.28±0.15) at.%, and* Co *(4.99±0.09) at.%. According to the scanning electron microscopy, the high entropy alloy is a polycrystalline material with the grain size ranging between 4 and 15 μm. The second phase particles are observed along its grain boundaries. Mapping methods are used to show that the grains are enriched with aluminum and nickel, while the grain boundaries contain chromium and iron. A quasi-homogeneous cobalt distribution is observed in the crystal lattice of the manufactured high entropy alloy. Tensile strength testing of the material shows its fracture by a transcrystalline rupture mechanism. The formation of brittle cracks occurs along the grain boundaries and point intersections, i.e., in places containing secondary phase inclusions. It is supposed that the higher brittleness of the high entropy alloy is caused by a nonuniform distribution of elements in the alloy microstructure and the presence of discontinuities of different shape in the bulk material.*

Keywords: high entropy alloy, Al–Co–Cr–Fe–Ni, wire arc additive manufacturing, deformation, tension, fracture surface structure.

INTRODUCTION

The approach to the creation of multicomponent alloys and compounds with the equal or comparable concentration of all components, ranks first in material physics of today [1, 2]. At the end of the 20th and early 21st centuries, the first publications appeared concerning the creation and comprehensive study of new high entropy alloys containing 5 or 6 principal elements in the amount of 5 to 35 at.% [3].

These materials, along with the parameters inherent to metal alloys, manifest a spectrum of unique properties that are typical for cermet, for example. Due to the difference in the atomic size of the elements in high entropy alloys, their crystal lattice is highly distorted, so they are characterized by low diffusion coefficients, corrosion resistance, higher ductility at low temperatures, and other properties useful for many promising functional materials [4].

The most widespread method of the high entropy alloy production is currently the vacuum arc melting, which has limitations in producing large-sized and shaped parts. Severe plastic torsion straining under pressure [5] and mechanical synthesis in planetary mills [6] provide a high level of mechanical properties. In recent years, more and more attention has been paid to additive manufacturing, which requires no molds for a part fabrication, since this

[1]Institute of Strength Physics and Materials Science of the Siberian Branch of the Russian Academy of Sciences, Tomsk, Russia, e-mail: yufi55@mail.ru; [2]Siberian State Industrial University, Novokuznetsk, Russia, e-mail: gromov@physics.sibsiu.ru; I.R.I.SS@yandex.ru; [3]Samara National Research University, Samara, Russia, e-mail: kirilloss@yandex.ru; ksv@ssau.ru; [4]Университет Вэньчжоу, г. Вэньчжоу, КНР, e-mail: chenxizhang@wzu.edu.cn.
Translated from Izvestiya Vysshikh Uchebnykh Zavedenii, Fizika, No. 9, pp. 103–108, September, 2021. Original article submitted January 11, 2021; revision submitted February 3, 2021.

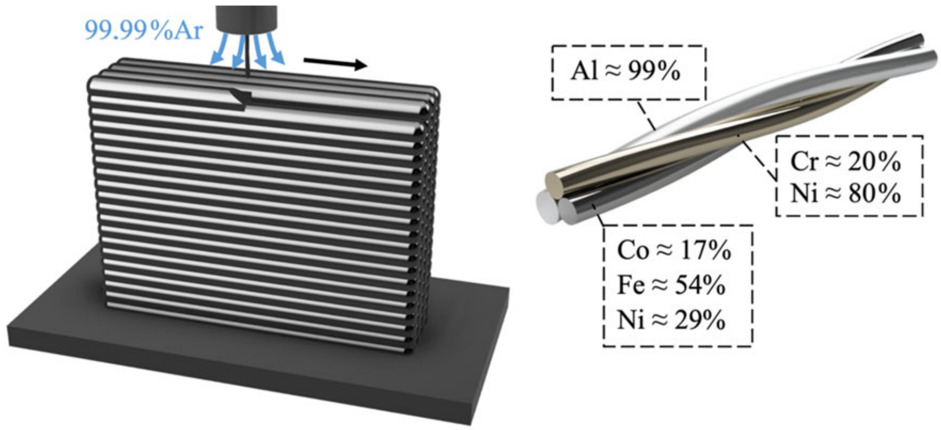

Fig. 1. WAAM-produced high entropy alloy specimen comprising layers of triple core wire (*a*), three-dimensional view of triple core wire (*b*).

process is the layer-by-layer formation of the material according to the given 3D model. Laser, electron beams, and electric arc are commonly used in such techniques as energy sources [3, 7].

Wire arc additive manufacturing (WAAM) has many advantages associated with the efficient deposition, high material ratio, low cost of equipment, *etc*. [8−11].

According to early research, the high entropy alloys of the Al–Co–Cr–Fe–Ni system have a set of high mechanical properties. Thus, the yield point for the $Al_{0.7}CoCrFe_2Ni$ alloy with the body centered cubic crystal system is 1223 MPa, whereas the fracture elongation is 7.9% due to the strengthening by the nanoscale *B*2-phase precipitation [12].

The two-phase $AlCoCrFeNi_{2.1}$ alloy possesses a striking combination of strength and ductile properties due to the nanoscale *B*2-phase and face centered cubic particle precipitations [13, 14]. The creation of the high entropy AlCoCrFeNi alloy with the improved strength and ductile properties is accompanied by the analysis of the different strengthening mechanisms such as solid solution and dislocation strengthening, grain boundary and twin strengthening, secondary phase strengthening [15−18].

According to Web of Science, over 5000 publications [1−3] are devoted to high entropy alloys, which report that the development of such alloys is a serious step toward the creation of metal alloys. A direct comparison of these works is rather difficult because of the difference in the composition of high entropy alloys, their thermomechanical processing, production process, and others. There is a process of accumulation and comprehension of information on structure, properties, deformation, stability, production processes, and scopes of application of high entropy alloys. The most detailed analysis of these issues is considered in review papers and monographs [1−4, 19−22].

The purpose of this work is to analyze the structure, elemental composition, and fracture surface of the high entropy AlCoCrFeNi alloy of the nonequiatomic composition produced by the wire arc additive manufacturing process.

MATERIALS AND METHODS

The AlCoCrFeNi alloy specimens were produced from triple core wire consisting of 99.95% aluminum (0.5 mm), nickel chrome (20% Cr and 80% Ni, 0.4 mm) and precision alloy (17% Co, 54% Fe and 29% Ni, 0.4 mm) (see Fig. 1). The high entropy alloy specimens were fabricated by the layer-by-layer deposition onto the grade 20 steel substrate using wire arc additive manufacturing (WAAM) in 99.99% argon gas. The operating parameters included 8 m/min wire feed speed, 17 V arc voltage, 0.3 m/min driving speed of burner, 250°C substrate temperature. The obtained high entropy alloy specimen was 60×140×20 mm in size and consisted of 20 layers in height and 4 layers in thickness, as illustrated in Fig. 1.

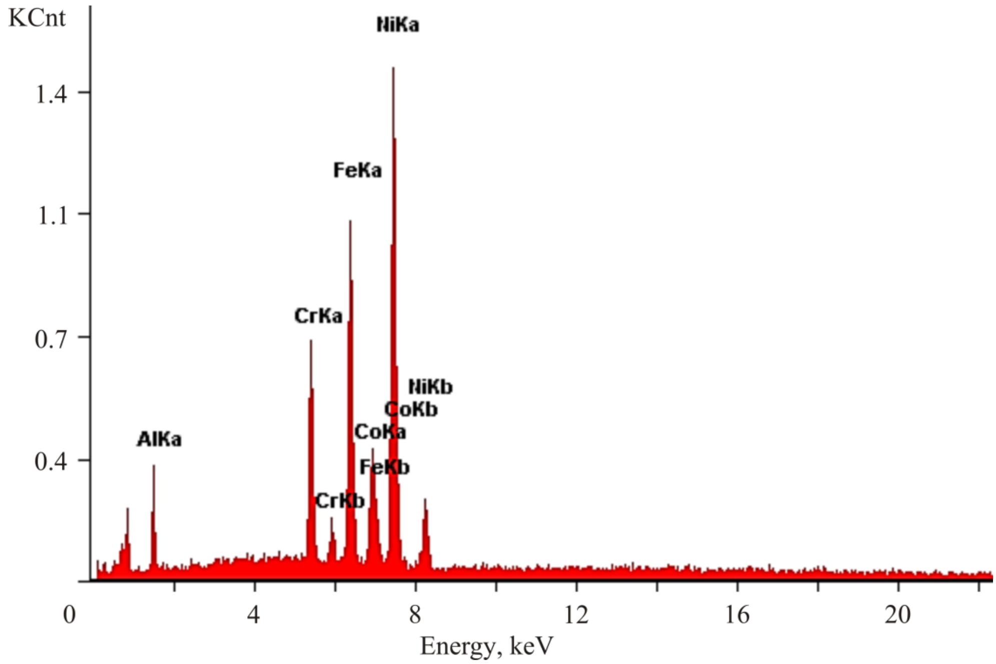

Fig. 2. Energy spectra and elemental composition of high entropy alloy.

The dog bone specimens manufactured in compliance with the Russian standard were subjected to tensile strength testing. Wire erosion was used to cut specimens of a desired shape normal to the direction of the layer deposition by using electrical discharges. Uniaxial tension tests were carried out on dog bone specimens 2.3 mm thick, 9.1 mm wide, and 16.0 mm long, using an Instron 3369 Dual Column Tabletop Testing System at 24°C and 2 mm/min testing speed and automatic recording the tension curve. The scanning electron microscopes Zeiss EVO 50 (Germany) and VEGA (Tescan, Czech) consisting of an integrated INCA (Oxford Instruments) energy dispersive X-ray (EDX) system was used to investigate the morphology of the specimens obtained. EDX was carried out over the specimen profiles. The elemental composition was averaged by 14 points. The distance between the points was 5 mm. The specified specimen structure was studied on polished sections etched in a reactive consisting of HNO_3 and HCL in a ratio of 1:3.

RESULTS AND DISCUSDSION

The polished sections of the alloy specimens show that the grain size varies between 4 and 15 µm. The secondary phase inclusions are observed along the grain boundaries and point intersections.

The energy spectra presented in Fig. 2, show the presence of aluminum, iron, chromium, and cobalt atoms in the material. According to the quantification analysis of the elemental composition, the principal elements of this alloy are Al (35.67±1.34) at.% and Ni (33.79±0.46) at.%. The rest elements have the following atom concentration: Fe (17.28±1.83) at.%, Cr (8.28±0.15) at.% and Co (4.99±0.09) at.%. Hence, this alloy can be called high entropy alloy of the nonequiatomic composition with the higher concentration of aluminum and nickel as compared to the equiatomic composition.

According to mapping methods, the WAAM process used for a fabrication of the high entropy alloy leads to a delamination of the ingot by its elemental composition. The grain boundaries are enriched with chromium and iron atoms (see Fig. 3*d*, *e*), while the grains contain nickel and aluminum atoms (see Fig. 3*b*, *f*). Cobalt atoms are distributed quasi-homogeneously in the bulk material, as shown in Fig. 3*c*.

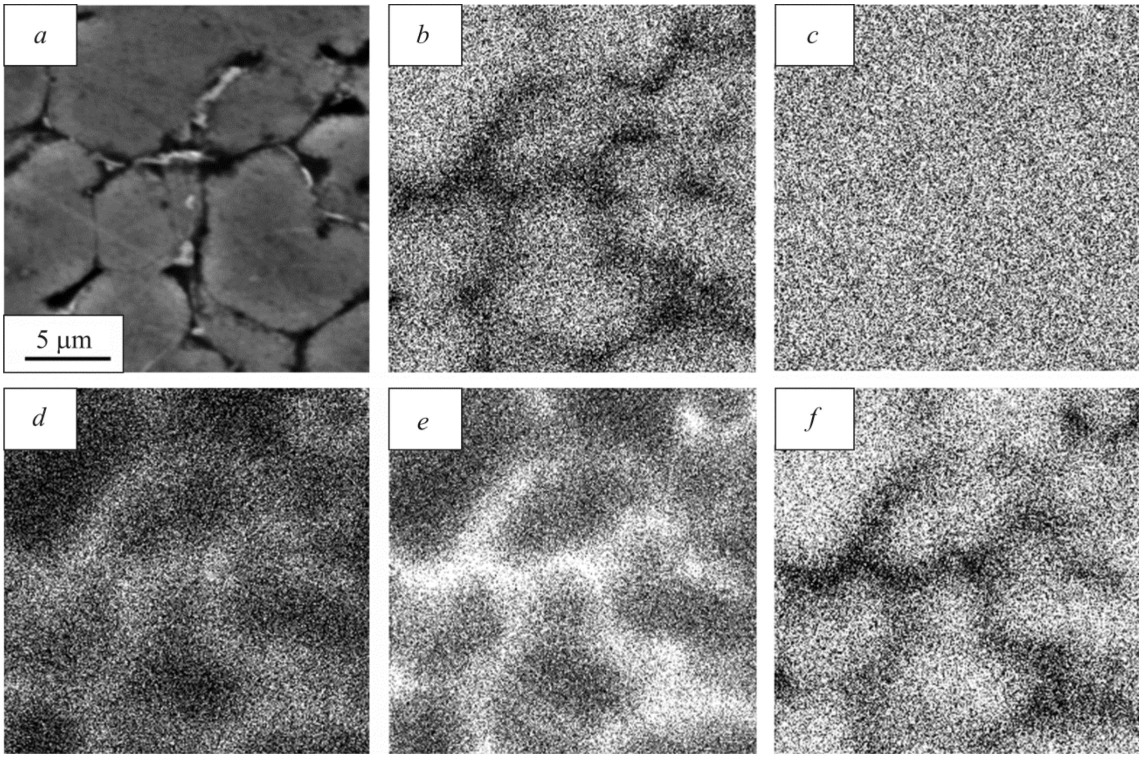

Fig. 3. Images of high entropy alloy: *a* – SEM image of polished section. EDX images of polished section for aluminum (*b*), cobalt (*c*), chromium (*d*), iron (*e*), nickel (*f*).

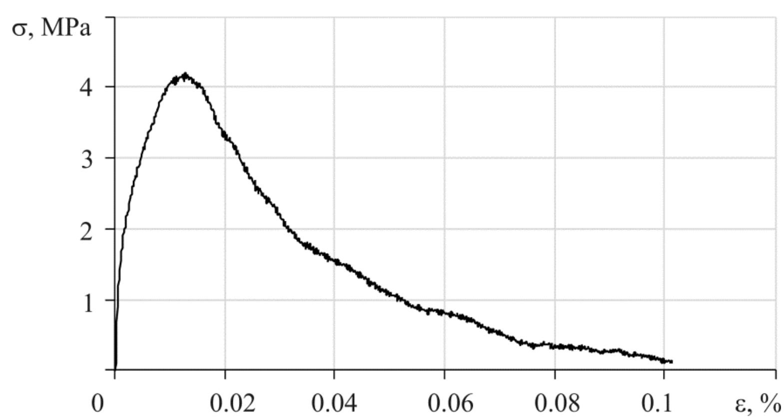

Fig. 4. Stress-strain curve of WAAM-fabricated high entropy alloy.

Figure 4*a* presents the stress-strain curve typical for the high entropy alloy tension. After tensile strength testing, this alloy possesses low strength and ductility owing to probably the presence of microcracks, micropores, and secondary phase inclusions in the dog bone specimen. The specimen shape indicates to its brittle fracture. It fractures along the plane positioned at an angle of 45 degrees to the axis of tension.

According to the scanning electron microscopy (SEM), the specimen fracture occurs by a transcrystalline rupture mechanism, i.e., by a plane, which is mostly a certain crystallographic plane for each grain of the material. Therefore, the fracture plane changes its orientation from grain to grain, thereby leading to a chaotic general view of the

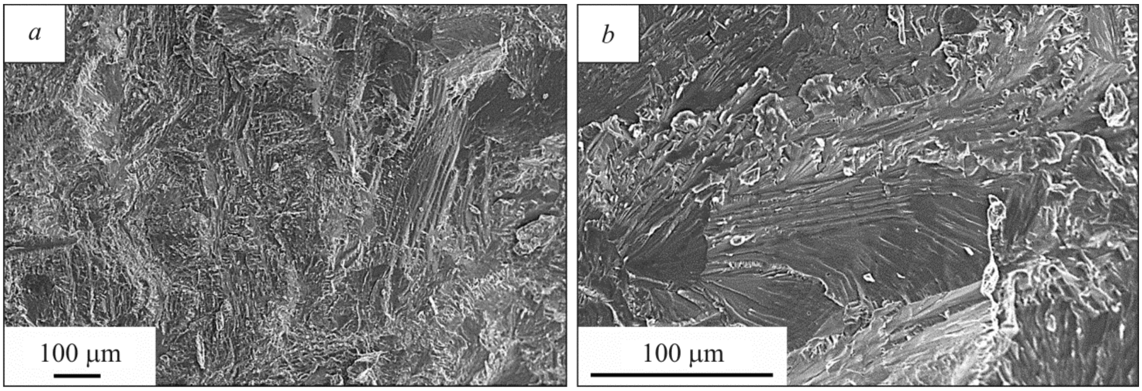

Fig. 5. SEM images of high entropy alloy fracture surface.

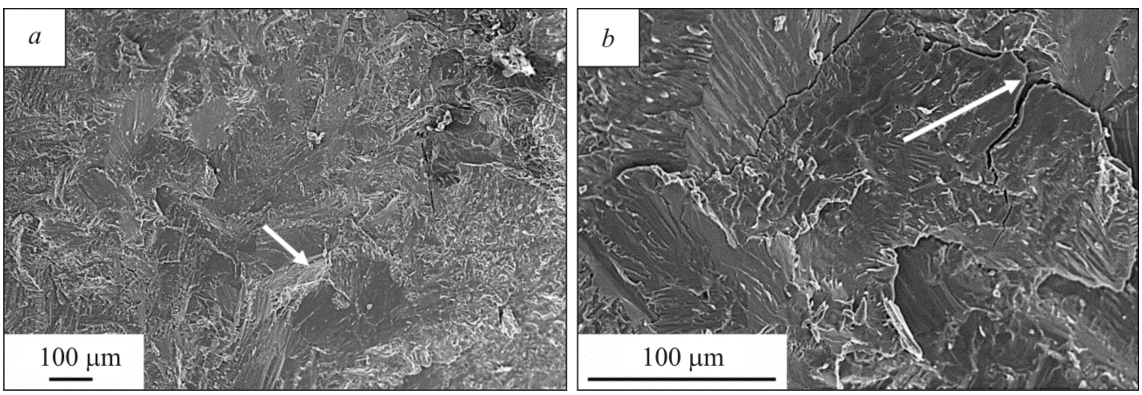

Fig. 6. SEM images of high entropy alloy fracture surface. Arrows indicate secondary phase particles, which induce localized specimen fracture (*a*) and a system of secondary cracks (*b*).

fracture surface, as presented in Fig. 5*a*. The grains are characterized by the river lines, which are the jogs between the different localized cleavage facets of the same cleavage plane (see Fig. 5*b*).

The main texture elements identified on the fracture surface by a cleavage, are the nuclei of the main and secondary cracks and the localized directions of the crack propagation (see Fig. 6*a*). The localized specimen fracture is caused by the secondary phase particles precipitated in the grain-boundary quadruple point intersection, as indicated by an arrow in Fig. 6*a*. The microrelief of the neighbor grains is different that indicates to their different crystallographic orientation. In Fig. 6*b*, a system of widely open secondary cracks is indicated by a white arrow, that means the material cracking in the direction perpendicular to the main fracture plane.

According to SEM observations, the specimen fracture surface has a great quantity of chaotically arranged micro- and macropores. Their size ranges from hundreds of nanometers to units of micrometers. This fact facilitates the material embrittlement.

The analysis of the fracture surface shows that the higher ductility of the WAAM-produced high entropy alloy can be caused by the material delamination by the elemental composition with the formation of the secondary phase inclusions along the grain boundaries, macro- and micropores of various size and shape, and microcracks appeared during the ingot fabrication.

CONCLUSIONS

The high entropy alloy system Al–Co–Cr–Fe–Ni of the nonequiatomic composition was obtained by using wire arc additive manufacturing. This was polycrystalline alloy, with secondary phase particles along the grain boundaries and the higher content of Al (35.67±1.34) at.% and Ni (33.79±0.46) at.% as compared to the equiatomic composition. SEM observations showed a nonuniform elemental distribution in the material microstructure, with the grains enriched with aluminum and nickel and the grain boundaries contained chromium and iron. Tensile strength testing of the material showed its fracture by a transcrystalline rupture mechanism. It was found that the formation of brittle cracks occurred along the grain boundaries and point intersections, i.e., in places containing secondary phase inclusions. The specimen fracture surface was characterized by micro- and macropores. Their size ranged from hundreds of nanometers to units of micrometers. It was supposed that the higher brittleness of the high entropy alloy was caused by the nonuniform distribution of elements in the alloy microstructure, the formation of secondary phase particles along the grain boundaries, and the presence of discontinuities of different shape in the bulk material.

This work was financed by Grant N 20-19-00452 from the Russian Science Foundation.

REFERENCES

1. E. P. George, W. A. Curtin, and C. C. Tasan, Acta Mater., **18**, 435−474 (2020).
2. Y. F. Ivanov, K. A. Osintsev, V. E. Gromov, S. V. Konovalov, and I. A. Panchenko, Steel Transl., **51**, No. 1, 27−32 (2021).
3. A. S. Rogachev, Phys. Met. Metallogr., **121**, No. 8, 733–764 (2020).
4. A. D. Pogrebnyak, A. A. Bagdasaryan, I. V. Yakushenko, and V. M. Beresnev, Russ. Chem. Rev., **83**, No. 11, 1027–1061 (2014).
5. A. Kilmametov, R. Kulagin, A. Mazilkin, *et al*., Scripta Mater., **158**, 29–33 (2019).
6. H. Cheng, Y. Xie, Q. Tang, *et al*., Trans. Nonferrous Met. Soc. China, **28**, 1360–1367 (2018).
7. Q. Shen and X. Kong, J. Mater. Sci. Technol., **74**, 136−142 (2021).
8. Y. Geng, S. V. Konovalov, and X. Chen, Prog. Phys. Met., **21**, No. 1, 26−45 (2020).
9. J. M. Wu, S. J. Lin, J. W. Yeh, *et al*., Wear, **261**, 513−519 (2006).
10. M. H. Chuang, M. H. Tsai, W. R. Wang, *et al*., Acta Mater., **59**, 6308−6317 (2011).
11. Y. F. Kao, T. D. Lee, S. K. Chen, *et al*., Corros. Sci., **52**, 1026−1034 (2012).
12. Q. Wang, Y. Ma, B. Jiang, *et al*., Scripta Mater., **120**, 85−89 (2016).
13. T. Xiong, S. Zheng, J. Pang, *et al*., Scripta Mater., **186**, 336−340 (2020).
14. R. John, A. Karati, J. Joseph, *et al*., J. Alloys Compd., **835**, 155424 (2020).
15. X. Jin, Y. Liang, L. Zhang, *et al*., Mater. Sci. Eng. A, **745**, 137−143 (2019).
16. Y. Liu, J. Chen, Z. Li, *et al*., J. Alloys Compd., **780**, 558−564 (2019).
17. M. Chen, L. Lan, X. Shi, *et al*., J. Alloys Compd., **777,** 180−189 (2019).
18. S. Qiu, X.-C. Zhang, J. Zhou, *et al*., J. Alloys Compd., **846**, 156321 (2020).
19. Y. Zhang, T. T. Zuo, Z. Tang, *et al*., Prog. Mater. Sci., **61**, 1–93 (2014).
20. D. B. Miracle and O. N. Senkov, Acta Mater., **122**, 448–511 (2017).
21. B. S. Murty, J. W. Yeh, S. Ranganathan, and P. P. Bhattacharjee, High-Entropy Alloys, Elsevier, Amsterdam (2019).
22. Y. Zhang, High-Entropy Materials. A Brief Introduction, Springer Nature (2019).